Journal of Aerosol Science 160 (2022) 105909

Contents lists available at ScienceDirect

Journal of Aerosol Science

journal homepage: www.elsevier.com/locate/jaerosci

Monodisperse droplets and particles by efficient neutralization of electrosprays

Antonio Carrasco-Munoz [a], Elena Barbero-Colmenar [a], Eszter Bodnár [a], Jordi Grifoll [a], Joan Rosell-Llompart [a,b,*]

[a] Department of Chemical Engineering, Universitat Rovira i Virgili, E-43007, Tarragona, Spain
[b] Catalan Institution for Research and Advanced Studies - ICREA, E-08010, Barcelona, Spain

ARTICLE INFO

Keywords:
Droplets
Droplet to particle
Electrospray
Electrohydrodynamic atomization
Gas phase ions
Corona discharge
Electrical charge
Polymer nanoparticles
Polymer microparticles
Curcumin

ABSTRACT

We present a new approach for micro- and nanoparticle production by in-situ charge reduction of electrospray droplets, which prevents their Coulombic instabilities and allow the efficient transport (extraction) of the particles. A unipolar ion source based on corona discharge generates a controllable ion flux of opposite polarity to the electrospray. The ions are introduced axially into the spray, while the Taylor cone is screened from the ions by an extractor ring electrode. Efficient and steady droplet discharge and extraction through an orthogonal aerosol-extraction tube was attained when the inlet of the tube was near the spray emission and the ring electrode, resulting in dramatic changes in droplets' trajectories. The best extraction conditions (highest filter collections) were associated with the best discharging (lowest residual electrical charge) and the most globular particles. The size distributions on the particles collected on the filters were monomodal and homogeneous, with small relative standard deviations (as small as 10.6%). The use of corona ions significantly expands the range of polymer concentrations over which globular particles with monomodal size distribution can be made by electrospray.

1. Introduction

Liquid aerosol to particle conversion is a versatile route for manufacturing nanoparticles (<100 nm), submicrometric particles (<1 μm), and small microparticles (1–10 μm) (Jafari et al., 2021; Malamatari et al., 2020; Vehring et al., 2020; Nandiyanto & Okuyama, 2011; Okuyama & Lenggoro, 2003). Making homogeneous droplets of the required sizes by liquid fragmentation, however, is difficult, as the conversion of a form of energy (e.g., pneumatic energy) into surface energy must be controlled at nanometric scales (Sosnik & Seremeta, 2015; Rosell-Llompart & Gañán-Calvo, 2008). Fittingly, electrospraying is capable of generating droplets in the micron- and submicron size ranges with size homogeneity and high energy efficiency (Rosell-Llompart et al., 2018; Gañán-Calvo et al., 2018). Therefore, interest in the electrospray route for producing small particles has been rekindled in various areas like ceramics (Tang et al., 2016; Suhendi et al., 2013), pharmaceutics/therapeutics (Ali et al., 2021; SverdlovArzi & Sosnik, 2018; Boda et al., 2018; Nguyen et al., 2016; Bock et al., 2012; Yurteri et al., 2010), nutraceuticals (Rostamabadi et al., 2021), and food encapsulation (Echegoyen et al., 2017).

Briefly, the liquid to be atomized is electrified, overcoming surface tension and causing the liquid-gas interface to adopt a conical

* Corresponding author. Department of Chemical Engineering, Universitat Rovira i Virgili, E-43007, Tarragona, Spain.
E-mail address: joan.rosell@urv.cat (J. Rosell-Llompart).

https://doi.org/10.1016/j.jaerosci.2021.105909
Received 6 September 2021; Received in revised form 27 October 2021; Accepted 31 October 2021
Available online 18 November 2021

shape. From the tip of such *Taylor cone* meniscus a steady jet is emitted, which breaks up into tiny droplets (Rosell-Llompart et al., 2018). This so-called *cone-jet mode* is sustained by continuously feeding liquid to the Taylor cone, typically through a capillary tube. Notably, the jet breakup often happens by the Rayleigh mechanism, which periodically releases droplets in repeatable sizes, while the high electrical charge on the droplets prevents their coalescence (Gañán-Calvo et al., 2018). In addition, droplet trajectories are controlled by the electrical field, making this technique very suitable for making thin coatings and particulate films on a counter electrode (Arumugham-Achari et al., 2013; Bodnár & Rosell-Llompart, 2013; Castillo et al., 2018; Hogan & Biswas, 2008; Hogan et al., 2007; Jaworek, 2007a; Jaworek et al., 2018; Kelder et al., 2018; Tang & Gomez, 2017).

On the other hand, making particles by electrospray in big amounts remains challenging mainly due to the electrical charge on the electrospray droplets. First, when making non-conductive particles collected as a particulate film on a substrate under the spray, the buildup of static charge on the film causes the progressive expansion of the electrospray plume (Bodnár & Rosell-Llompart, 2013). Meanwhile, micro-discharges in the film could develop, damaging the particles (at least hypothetically, as the existence of micro-discharges inside electrospray films has not been directly observed) (Uecker et al., 2010). Second, when multiplexing electrosprays, the electrostatic repulsion between different sprays limits the scalability of the process (Sochorakis et al., 2019; Almería et al., 2011; Deng et al., 2006; Bocanegra et al., 2005). Thirdly, the charged droplets attain fast speeds in the high electrical field (of order m/s), often leading to incompletely dried particles on the collection electrode, even forming continuous films. This is more likely to happen with low volatility solvents (e.g., DMF), larger droplets (several micron in diameter, commonly encountered), and multiplexed systems, where the sprays are not allowed to expand much when Taylor cones are close to each other (Sochorakis et al., 2019).

A fourth issue caused by the high electrical charge on the droplets is Coulombic instabilities (CIs), which droplets experience while evaporating, when the *destabilizing* electrical stress on the droplet's surface (where the net charge resides) grows to a point at which it exceeds the *stabilizing* capillary tension stress, which grows slower (Duft et al., 2003; Saville, 1997; Gomez & Tang, 1994). In the context of particle manufacturing, CIs are usually undesired, as they lead to non-spheroidal (elongated or filamentous) particle shapes and mixed sizes (Li et al., 2007). Only under specific conditions can CIs be prevented, by the early formation of a solid shell on the evaporating droplet (Bodnár et al., 2018; Almería et al., 2010; Bock et al., 2012). In the case of polymeric solutes, this strategy works only within a narrow range of solute concentrations (Meng et al., 2009), while sometimes only working in one region of the spray (due to even slight differences in droplet size and charge) (Bodnár, 2016). Another way an early shell can form is by uptake of a non-solvent vapor, e.g., water vapor for some solvent-polymer systems (Bodnár et al., 2018). However, this often leads to irregular porous structures, which may not be desirable.

Several works aimed at making small particles by electrospray have attempted the reduction of the droplets' charge by combining them with gas-phase ions of opposite charge. This was done by several approaches: (i) bipolar ions created by radioactive sources (Lenggoro et al., 2000), (ii) unipolar ions created by corona discharges (Yurkstas & Meisenzehl, 1964; Meesters et al., 1992; Cloupeau, 1994), and (iii) bipolar ions created using a double corona system (Mustika et al., 2021). The second approach was the most popular, having been attempted in producing (1) inhalation aerosols for drug delivery (Noakes et al., 1989; Zimlich et al., 2002; Davies et al., 2005), (2) pharmaceutical particles (Almería & Gomez, 2014; Xie & Wang, 2007; Ciach, 2006, 2007; Xie; Marijnissen & Wang, 2006; Xie, Lim et al., 2006; Davies et al., 2005; Zimlich et al., 2002; Ijsebaert et al., 2001; Tang & Gomez, 1994), and (3) ceramic powders (Rulison & Flagan, 1994; Tang et al., 2017). All these electrospray works aim at generating small particles with minimal material loss.

In none of the abovementioned works combining electrosprays with corona ions to make particles could we find data on the droplet discharging efficiency, the particle morphology changes, or their dependence on the independent variables of the problem (electrode geometrical parameters, corona conditions, electrospray conditions, etc.). Nor have the ion losses and droplet losses typically been investigated, despite their importance. All these important questions must be answered to improve and optimize electrospray-corona systems. One recent exception is Mustika et al. (2021), focused on producing low-charge airborne nanoparticles by electrospraying nanoparticle suspensions, although their particle losses are too high for our purpose. System configurations leading to high efficiency remain to be demonstrated. In addition, such data should be useful for informing numerical simulations on these systems (Higuera, 2016; Khalifehei & Higuera, 2020).

Therefore, in this work, we have carried an experimental study to address some of these questions in the context of producing solid particles as residues of electrospray droplets containing non-volatile solutes. We have aimed to (i) determine whether it is possible to discharge electrospray droplets emitted from a single Taylor cone in a controlled, stable way, without compromising the electromechanical stability of the Taylor cone, (ii) show that it is possible to efficiently transport and collect the generated particles far from the spray region, and (iii) identify configurations and operating conditions in which the Coulombic instabilities of the droplets are avoided.

Interestingly, corona ions have also been used to charge-reduce droplets and analyte ions in electrospray ionization mass spectrometry (ESI-MS) (Fenn, 2003), an analytical technique by which solutes (importantly, proteins and large biological entities) can be transformed into gas-phase ions and be weighed by standard mass spectrometers (Ebeling et al., 2000, 2001; Campuzano & Schnier, 2013; Bornschein & Ruotolo, 2015). However, as the aim in these studies is ion analysis, their optimal configurations and chemical compositions do not apply to the goal of particles production.

2. Materials and methods

2.1. Materials

All the chemical reagents were used as purchased, without further purification. Polystyrene (PS) (CAS Number 9003-53-6, weight-average molecular weight (M_w) of 35 kDa), methyl ethyl ketone (MEK) also known as butanone (ACS grade, CAS Number 78-93-3,

residue on evaporation 0.0020%), ethylene glycol (reagent grade, CAS Number 107-21-1), curcumin (CUR) (99% purity, CAS Number 458-37-7, 368.38 g/mol), and polyvinylpyrrolidone (PVP) (CAS Number 9003-39-8, M_w of 40 kDa) were purchased from Sigma Aldrich. Sodium chloride (NaCl) (ACS grade, CAS Number 7647-14-5), ethanol absolute (ACS reagent grade, CAS Number 64-17-5), and acetone (ACS reagent grade, CAS Number 67-64-1) were purchased from Scharlau. Synthetic dry air 99,998% purity was purchased from Carburos Metálicos, Spain (20.9% ± 1% O2 with 3 ppm M of H2O, 0.2 ppm M of THC and 1 ppm M of CO and CO2, the rest being N2).

2.2. Solution preparation and characterization

We have used three different liquid solutions: one with a nonvolatile solvent (EG) and two based on polymer solutions in volatile solvents (PS in MEK, and PVP in ethanol:acetone 1:1 by volume). For the ethylene glycol solutions, a stock solution was first made by dissolving 21 mg of NaCl in 75 ml of ethylene glycol and stirring the solution overnight. This initial solution was then diluted under stirring to obtain 0.007% w/v and 0.0007% w/v solutions. For the polymer containing solutions, the necessary mass of solvent was added to a given mass of solute, followed by magnetic stirring overnight. However, PS solutions at 3% w/w were prepared by dilution of a 5% w/w PS in MEK prepared in this way. A 5 ml Gay-Lussac pycnometer was used to measure the density of some solutions. We measured the electrical conductivity with a portable conductivity meter (CRISON 35) using a glass-body probe (CRISON 50 61). The solutions concentrations and properties are given in Table 1.

2.3. Electrospray-corona apparatus and particle extraction system

The electrospray and corona subsystems were housed in a chamber for gas ambient control (Fig. 1a). The chamber consisted of a fixed black Delrin® platform (to which the electrospray subsystem and corona ion source were mounted), a Delrin® base frame sitting on the platform, a black Delrin® wall for all the connections (electrical, gas, and liquid supplies, particle sampling and extraction, etc.) which is screwed to the base frame, and a removable glass urn made of three glass panels (175 × 130 × 1.8 mm) and a glass top (135 × 135 × 3 mm) (Fig. SI.1). The urn's edges sit on rubber seals, so the urn can be lifted easily. During electrospraying, the urn was in place (except where noted) and synthetic dry air was supplied to the chamber at 4.4 lpm. The air exited the chamber through the particle extraction tube and passed through the collection filter, as well as through a port exhausting to a remote fume hood. The chamber gas inflow was set to maintain about 5–10 Pa in the chamber, sensed by a Magnehelic differential pressure meter (cat. no. 2000-125 Pa C). Meanwhile, the relative humidity in the chamber (*RH*) was monitored using a Vaisala HM34 m probe inserted through the Delrin® lateral wall.

Electrospray subsystem. The electrospray capillary was made of 304 stainless-steel capillary tubing (Tubos Capilares, Spain; 160 μm ID, 400 μm OD), square cut to a 30 mm length, and polished on its exit end. It was centered inside a square-ended glass tube (1.16 mm ID, 2.00 mm OD) and its protrusion varied (~0.5 mm in the particle generating experiments, and longer in the ethylene glycol experiments). When spraying polymer solutions, a gentle sheath flow of solvent-saturated gas (synthetic air) flowed through the glass tube, around the capillary, at a typical plug-flow speed of 80 mm/s, to prevent polymer precipitation at the Taylor cone (TC) meniscus caused by solvent evaporation. The use of such flow was first suggested by Larsen et al. (2004) but is not widely practiced, although we often find it necessary when making small particles by electrospray (Bodnár et al., 2013, 2018). The liquid solution was fed to the capillary by a syringe pump (Harvard Apparatus PHD 2000) from a glass syringe (Hamilton® syringe, 1000 series GASTIGHT®, 1 ml) connected to a 27-gauge × ½'' hypodermic needle fitted to a PTFE capillary tubing (Teknokroma, 360 μm ID, 580 μm OD) into the electrospray capillary.

A ring electrode (5 mm ID, 1 mm thickness) was placed beneath the electrospray capillary in nozzle-to-ring down configuration (Fig. 1a and b). This configuration is commonly used in electrospray practice to provide electrostatic shielding (Jaworek, 2007b; Cloupeau, 1994). The voltage difference between the capillary and the ring established the electric field that is needed to generate the electro-atomization. Here, the ring has the important additional benefit of shaping the electrical field to guide the ions to interject the droplets' trajectories.

Corona ion source. In conceiving the ion source, we hypothesized that attaining efficient discharging required injecting the ions coaxially with the spray. In addition, we hypothesized that the ion and spray currents must be alike (though not necessarily equal). Since corona currents easily exceed electrospray currents by an order of magnitude or more, an orifice plate ("corona extractor") was

Table 1
Properties of the solutions.

Solution code	Solutes and concentrations	Solvent	Electrical conductivity, S/m	Solution density, g/cm^3
007EG	NaCl: 0.007% w/v	Ethylene glycol	9.6×10^{-4} (24.5 °C)	1.116 (25.0 °C)*
0007EG	NaCl: 0.0007% w/v	Ethylene glycol	1.13×10^{-4} (24.7 °C)	1.116 (25.0 °C)*
3PS-MEK	PS: 3% w/w	Butanone	6.9×10^{-5} (23.3 °C)	0.807 (24.8 °C)
1CUR-5PVP	PVP: 5% w/w Curcumin: 1% w/w	Ethanol/acetone (1:1 v/v)	1.43×10^{-3} (24.0 °C)	0.815 (20.5 °C)
0.1CUR-5PVP	PVP: 5% w/w Curcumin: 0.1% w/w	Ethanol	1.21×10^{-3} (21.6 °C)	0.790 (20.0 °C)*

* Not available. Value shown is for the pure solvent.

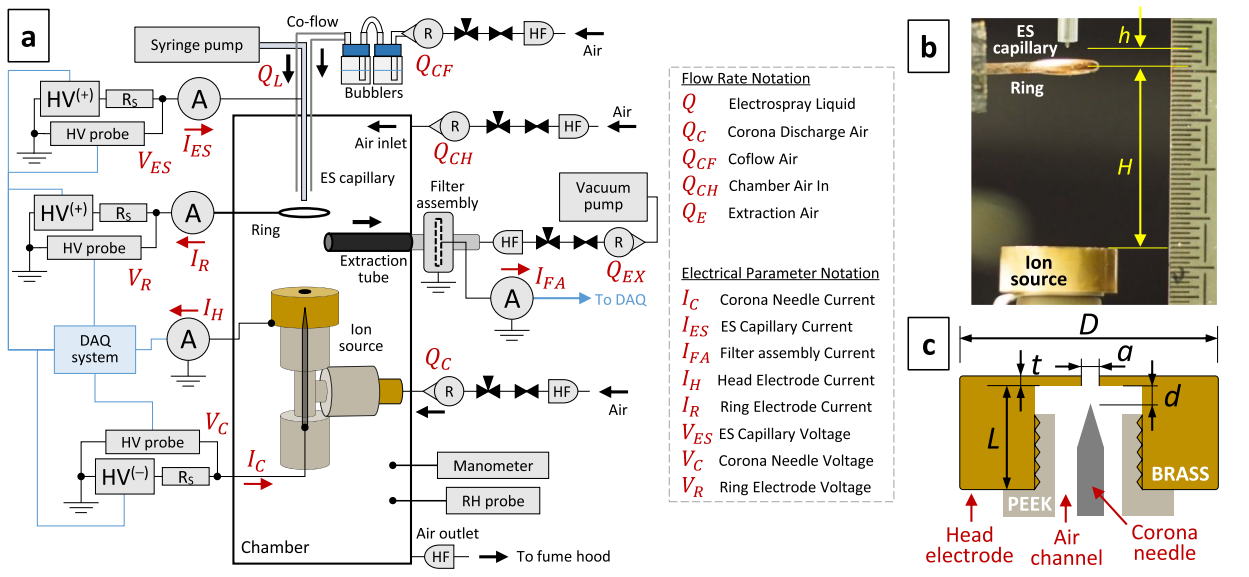

Fig. 1. Setup used for generating ions and electrospray droplets. (a) System schematic comprising electrospray with coflow, unipolar ion source, extraction tube with filter assembly. (b) Photography of the discharge zone with height parameters. (c) Cross section of top of corona subsystem (a = 2.0 ± 0.1 mm, t = 0.4 ± 0.1 mm, d = 1.2 ± 0.1 mm, D = 12.0 ± 0.5 mm, L = 4.0 ± 0.5 mm). Acronyms: DAQ = Data acquisition; HV = high voltage; HVPS = HV power supply; A = ammeter; HF = HEPA filter; R = rotameter; R_S = safety resistor (250 MΩ).

placed in front of the corona needle. This limited the ionic current passing to the spray region. In the context of particle production by electrospray and corona discharging, an intermediate electrode was previously used also by Tang et al. (2017), and briefly by Cloupeau (1994). Therefore, the home-made unipolar ion source consisted of a corona discharge needle (Alfa Aesar, tungsten 1.5 mm diameter rod, sharpened to 15 μm tip radius with 32° total angle) housed inside a modified tee connector (IDEX P-714 Low-Pressure Tee Assembly, Natural PEEK), capped with an Earth-grounded "head electrode" which coaxially had an orifice for ion extraction into the spray region (Fig. 1a and c). The voltage difference between the corona needle and the head electrode established the electric field to sustain the corona discharge. Synthetic dry air was continuously fed to the corona discharge region at a low flow Q_C as shown in Fig. 1a (at 13.3 ml/min, corresponding to plug-flow gas speed at the exit orifice of 71 mm/s). However, this flow did not significantly affect the current of ions available to the spray.

The electrospray capillary, the ring electrode, and the corona needle were each connected to a channel of an Ultravolt high voltage power supply (HVPS) (HVRACK-4-250-0032) through a high voltage-rated 250 MΩ resistor, used for user safety. For the first two, we used voltage regulation, whereas for the corona needle we used current regulation. The electric potential at each electrode was continuously monitored by respective HV probes (Testec, TT-HVP-40, 1 GΩ), and the electrical currents flowing through these electrodes and through the corona head electrode were measured inline by battery powered nano-ammeters (home-made current-to-voltage opamp-based designs). The directions of the reported currents are given in Fig. 1a. The outputs from the ammeters, voltage, and current monitor from the HVPS, and from all the HV probes are fed to a National Instruments PCI-6221 DAQ card on a desktop computer.

Particle collection systems. Discharged droplets/particles from the spray were extracted into an antistatic tube (SCAT conductive plastic tube, 4 mm ID, 6 mm OD, 6 cm length) inserted through the chamber Delrin® lateral wall. This extraction tube was connected to a Swinny filter holder made of either metal (stainless steel) or plastic (polypropylene). The holder housed a Whatman glass microfiber filter (a 25 mm diameter filter with 1.6 μm pore size for PS aerosols, and either a 25 mm × 1.0 μm or a 13 mm × 1.6 μm filter for PVP-CUR aerosols). The extraction gas flow was provided by a vacuum pump (Laboport N86KT.18). The filter assembly (filter holder plus filter) was placed inside a purpose-made Faraday-cage, whose inner metal shell (for plastic filter holder) or the metal filter holder is connected to a Keithley 6485 picoammeter to monitor the residual electrical charge current carried by the electrospray droplets to the filter assembly. For comparison, in the absence of corona ions, electrospray particles were also collected on silicon wafers (Si-Mat, Germany, <100>, 525 μm thickness, P/Boron, 1–30 Ω cm). A silicon wafer fragment sitting on top of a thin steel ruler (165 × 13, mm) was placed underneath the spray, on top of the corona head electrode. The ruler was Earth-grounded and was inserted through a slit on the chamber Delrin® lateral wall, and the Si wafer remained on the ruler all the time during the collection.

Illumination and photography. Two cameras (Olympus PEN E-PL7 and Olympus PEN EP-1)) were used for photographing (i) the electrospray plume with a Nikkor macro lens (60 mm, 1:2.8) under darkfield illumination using a single white LED spot lamp, and (ii) the Taylor cone with an Edmund Optics VZM 450i zoom imaging lens under brightfield illumination to verify the cone-jet mode in all the experiments (Rosell-Llompart et al., 2018).

2.4. Electrospray discharging protocol

Stable combination of the electrospray with the ions and with the extraction gas flow relies on balancing the right electrode voltages and the right flow speeds. To achieve a stable balance, we used the following protocol with a closed chamber. Initially, with the extraction tube kept far from the spray axis, we set both the chamber airflow in (which vents to the fume hood) and the corona discharge airflow. With the corona head electrode covered, we established the electrospray in cone-jet mode and the corona discharge. For the first, we set the voltage difference between the ES capillary and the ring electrode at their approximate final values (known from previous practice runs), and then we feed the liquid solution through the capillary (with the coflow on when in use). The ES capillary and ring voltages were chosen to be high enough to drive the droplets towards the head electrode (kept at Earth-ground), rather than back toward the ring (data shown later). The direct currents were monitored at the electrospray capillary (I_{ES}), at the ring (I_R), and at the corona head (I_H) (Fig. 1). Any positive ring current at this stage is interpreted as due to droplet deposition.

Next, after both the electrospray and the corona discharge were stable, the vacuum pump was turned on to start the extraction airflow. Within a few seconds, the head electrode was uncovered to allow the passage of ions through the head electrode orifice into the spray region. This disturbed the spray, which typically became a floating dense aerosol cloud. At the same time, typically, the Taylor cone shrunk a bit. If a change to multi-jet spraying mode happened (Rosell-Llompart et al., 2018), we regained stability in the cone-jet mode by lowering the ES capillary voltage. (Therefore, to prevent that the cone-jet would become unstable when the ions were introduced into the system, we started with a slightly elongated cone shape.) Often, we recorded a finite current at the ring electrode ($I_R < 0$), which is due to ion collection, and an increase in the ES capillary current (I^*_{ES}) (Fig. 1a).

Immediately after, the extraction tube was approached to the aerosol cloud at the desired location. Often this distorted the discharging process, so, meanwhile the tube was positioned, the voltages were readjusted to maintain a steady and stable process (spray outline, cone, currents). We assumed that the droplet extraction was maximized when we saw the whole aerosol entering the tube. The 'dead' time between the moment when the corona orifice was uncovered (to admit ions into the spray region) and the moment when we started the timer (needed for establishing the particle collection time) was very small (typically one or a few seconds), and negligible compared to the total particle collection time.

2.5. Particles' collection and charge-reduction efficiencies

The particle masses collected on the filter assembly (FA) m_{FA} and on the extraction tube m_{tube} (which includes the connector to the FA) were obtained by the weight differences before and after particle collection determined with a 5-digit analytical balance (Mettler Toledo XS205 Dual Range). The *extracted particle mass* was computed as $m = m_{FA} + m_{tube}$ and the *extraction efficiency* as:

$$\eta = m/m_{ES} \tag{1}$$

where m_{ES} is the mass of polymer in the electrosprayed solution, which we computed from the polymer mass fraction in the solution C_p, the infusion flow rate Q, the solution density ρ, and the collection time t as $m_{ES} = C_p \cdot Q \cdot \rho \cdot t$. The extraction efficiency can be decomposed as the sum of the contributions from the filter assembly $\eta_{FA} = m_{FA}/m_{ES}$ and from the extraction tube $\eta_{tube} = m_{tube}/\ m_{ES}$:

$$\eta = \eta_{FA} + \eta_{tube} \tag{2}$$

The residual electrical charge current carried by the electrospray droplets to the filter assembly I_{FA}, time-averaged over the collection time, is used to determine the *discharge efficiency* ζ defined as the fractional reduction in the initial charge of the droplets which, after combining with the ions, lead to particles collected on the filter holder. Such efficiency is computed as:

$$\zeta = 1 - \frac{< I_{FA} >}{I_{ES} \cdot \eta_{FA}} \tag{3}$$

where I_{ES} is the electrospray current, and $(I_{ES} \cdot \eta_{FA})$ is an estimate of the initial electrospray current associated with the droplets which correspond to the particles on the filter. "$< >$" means time averaging (necessary when the I_{FA} signal changed with time). A value of 1 for ζ would mean that the aerosol collected on the filter holder is overall electrically neutral. The current in the Faraday-cage electrometer was not stable when plastic filter holders were used. Therefore, we report only the ζ values for a metal filter holder.

2.6. Particle morphology and size characterization

The particles were imaged by scanning electron microscopy (SEM) (FEI Quanta 600) to determine particle morphology and size. After they were collected, on filters or on Si wafers, they were stored in a dry ambient until imaged, done typically on the same or the following day. Before being imaged, particles collected on the filters were either transferred to the carbon tape of the SEM sample holder by gently dabbing the tape on the particle collection, or by sticking a cut piece of the filter membrane with particles onto the C tape. Prior to imaging any samples, they were coated with a ~27 nm Au layer (30 mA, 180 s) in a sputter coater (either a Quorum Q150R ES or a Quorum Q150T S plus). The particle size distribution was determined by manually sizing particles in the SEM images using ImageJ software (version 1.53e).

3. Results and discussion

We have used a non-volatile solvent, ethylene glycol, to investigate the role of the various parameters on the generation of ions and of droplets separately (#3.1), and the effects of the ions on the spray plume shape for a low-volatility solvent without the presence of solutes (#3.2). This absence of solutes simplifies the system under study. Otherwise, accumulation of solutes on electrode surfaces could change the electrical field over time. Finally, we apply the developed system to the production of two different types of particles in example systems based on polystyrene (PS) solutions (#3.3) and polyvinylpyrrolidone-curcumin (PVP-CUR) solutions (#3.4).

3.1. Electrostatic control of ion and droplet trajectories

The corona head acts as the counter electrode to the corona needle, thus collecting most of the ions emitted from the corona, and allowing only a small fraction of the corona current to pass through its orifice and become available to interact with the electrospray droplets. This current fraction must be small because corona currents (a few μA) far exceed electrospray currents (tens of nA). The capture of ions by the droplets (Fig. 1) depends critically on the droplets' and ions' trajectories, thus on the electrical field, which depends on the electrodes' voltages and geometries.

First, in the absence of spray, we studied how sensitive the ionic current passing through the head electrode orifice into the spray region (I_{Ext}) is to both the corona current (I_C) and the ring voltage (V_R). In these experiments, the electrospray capillary was removed. Also, to ensure the trapping of any central ions, the ring was covered with a metal disc (12.7 mm diameter). These geometry changes allowed us to determine I_{Ext} without elimination of the essential elements. Fig. 2 shows that I_{Ext} is (i) weakly dependent of the corona current, and (ii) can be regulated by means of the electrical field E_{Ext} in the region *outside* of the corona device through V_R, where $E_{Ext} \sim V_R/H$.

Fig. 2 shows that the electrical field outside of the corona device (head electrode) strongly influences the ion current available to discharge droplets. Note that in the absence of a ring electrode, it would be challenging to control the Taylor cone stability. A single voltage difference (between the capillary and the head electrode) would be simultaneously controlling: (1) the droplet generation near the Taylor cone at the capillary exit, and (2) the ionic current available for droplets' discharging. Such configuration has, in fact, been proposed in the prior literature (see Introduction). The (better) configuration used here includes a ring electrode, and this allows independent control of (1) and (2). Its voltage difference with the head electrode (here, V_R) governs the trajectories of ions and droplets in the space between, while its difference with the electrospray capillary ($\Delta V = V_{ES} - V_R$) governs the formation of the Taylor cone.

Such independent control is demonstrated by Fig. 3. In Fig. 3a, the electrospray was monitored in the absence of corona, while varying both V_R and V_{ES} at constant difference (ΔV). We found near constancy for the electrical current at the capillary I_{ES} as shown in Fig. 3b. This demonstrates that the droplet generation process was affected minimally, if at all. Meanwhile, the electrospray droplet trajectories experienced big changes, as is evident from the spray appearance (Fig. 3c). Through the voltage scan, also the head electrode and ring currents varied widely, for low enough values of V_R (Fig. 3b). The former decreased and the latter increased as part of the spray was diverted toward the ring, while both currents consistently add up to the electrospray capillary current, as expected.

Fig. 3d plots the ring current I_R versus ring voltage V_R from Fig. 3a and b. This current is associated with droplet deposition on the ring due to droplet flying-back toward it, causing liquid accumulation over time on the ring electrode (visible in Fig. 3c). The accumulated liquid probably attracted electrical field lines, thus reinforcing the flying-back. We believe this to be the reason for the increase in ring current over time as observed in Fig. 3d, along with a shift in the V_R at which the flying-back starts (from ~1.3 to 1.5 kV).

3.2. Discharging of ethylene glycol electrosprays

The droplet neutralization process requires a suitable combination of three elements: 1) the electrospray plume, 2) the ion plume, and 3) the gas flow field responsible for removing discharged droplets (into the extraction tube). We have qualitatively investigated

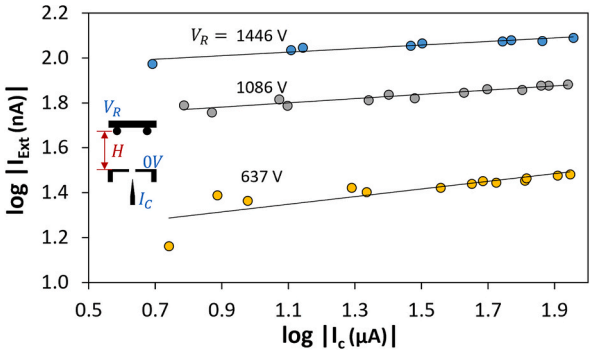

Fig. 2. Log-Log plot of extracted ion current I_{Ext} (<0) measured at the counter electrode (ring plus disk, as shown in the inset) versus the corona current I_C, at varying ring voltage, V_R (values displayed). ($H = 17.0$ mm $Q_C = 20$ ml/min). Electrode diagram is included, showing the absence of electrospray capillary and the covering of the ring with a disc. Lines are power-law fits.

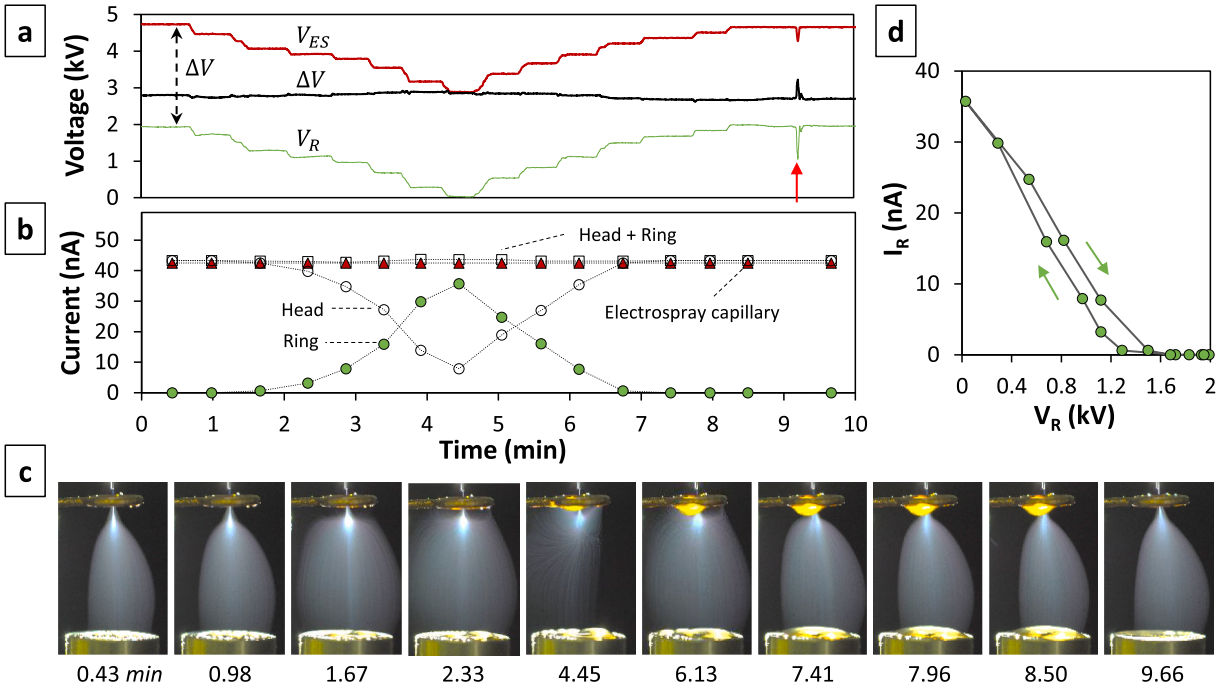

Fig. 3. Experiment showing the effect of the electric field between ring and counter electrode (without ions) on the electrospray plume (for solution 0007 EG). (a) V_R and V_{ES} versus experiment time, varied with $\Delta V \sim 2.8$ kV (also shown). (b) Electrode currents I_{ES}, I_R and I_H, and the sum of these two, versus experiment time. (c) Snapshots corresponding to some of the current measurements. The last photo was made after (at time shown with an arrow in (a)) the liquid accumulated on the ring and corona head was wiped with a cloth, without interrupting the spraying. (d) I_R as a function of V_R throughout the experiment. ($H = 17.0$ mm, $h = 1.3$ mm, $Q = 5$ µl/min)

how the ions influence the spray plume shape using non-volatile (ethylene glycol) solutions in the presence or absence of extraction flow. Fig. 4 illustrates different situations in which the electrospray is electrically discharged, or not, by an ion stream having similar electric current to the electrospray. In Fig. 4a ions and extraction flow are absent, and the spray adopted a typical plume shape, in which the droplets follow predictable trajectories which are close to the electrical field lines (Arumugham-Achari et al., 2013; Higuera, 2012). In Fig. 4b, the addition of corona ions leads to chaotic wavy motions of the spray plume when the extraction tube is still far away from the spray. (Several videos are shown in the Supplementary Information file.) The droplet trajectories did not follow the electrical field lines, as they are convected by spurious gas currents. This proves that most of the droplets lost most of their initial charge. A similar situation was found when a ring electrode is not present (videos 2 and 3 in SI file). However, the use of a ring made it easier to control the system, as already mentioned for the ions and droplet separately.

In Fig. 4c, the extraction flow (set by the extraction tube) was brought near the spray region, cancelling the chaotic motion as the droplets were suctioned into the tube. In this case, the droplets followed nearly steady trajectories, which depart strongly from the electric field lines (which are nearly the same as the droplet trajectories in Fig. 4a). If, while the flow was on, the ions were turned off, the extraction flow became uncapable of suctioning the spray into the tube, as demonstrated in Fig. 4d. (They moved slightly away from the extraction tube, indicating electrostatic repulsion due to an initial accumulation of charged droplets.)

From these tests, we conclude that the droplets' trajectories are very different when the ions are present than when they are not. Therefore, the capture of ions by the droplets is very efficient, enough to greatly reduce their initial net electrical charge. The droplets follow mostly the electrical field lines when the ions are not present, whereas they follow closely the gas streamlines when they are discharged (or significantly discharged). Interestingly, this observation allows us to roughly estimate the electrical mobility of the droplets before neutralization. As the air speed at the inlet of the tube v_{tube} is 5.5 m/s and the electrical field strength in this region is of the order of $V_R/OD_{Ring} = 1.0$ kV/7 mm $= 1.4 \times 10^5$ V/m, the droplets' initial electrical mobility μ (speed/field strength) must be of the order of $v_{tube}/(V_R/OD_{Ring})$, namely (5.5 m/s)/(1.4×10^5 V/m) $= 4 \times 10^{-5}$ m^2/(V·s).

In Fig. 4e, the ions had been turned on again and the electrospray aerosol was extracted into the extraction tube as before (Fig. 4c), demonstrating that the process is reversible. Note that here the tube was very close to the spray axis, and the extraction was still robust.

In sum, the spray suffered dramatic changes when ions were introduced (with similar electrical current), and the proximity of the gas flow at the inlet of the extraction tube was critical to attain steady droplet discharging and extraction.

3.3. Polystyrene particles from discharged PS/MEK electrosprays

To demonstrate the use of our charge reduction method to produce particles we have chosen a solution of 3% w/w of 35 kDa PS in

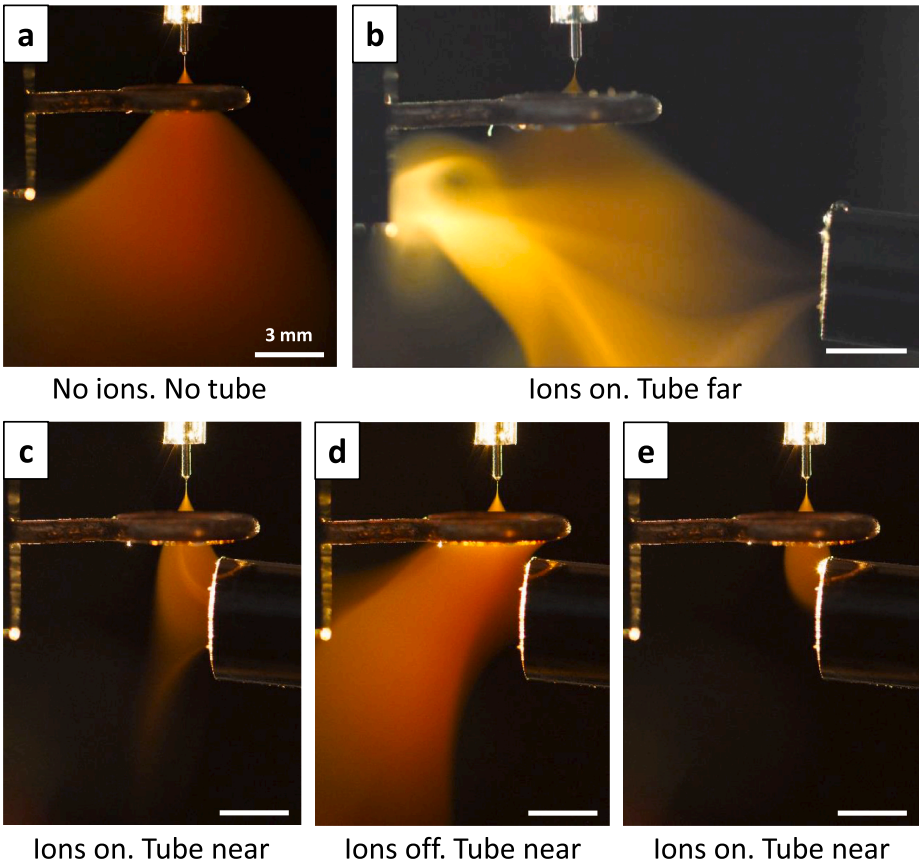

Fig. 4. Ethylene glycol electrospray (solution 007 EG) (a) in absence of extraction flow and ions, and (b–e) in presence of extraction flow under different situations: (b) Exposed to corona ions, but tube located far (for which the discharged aerosol does not follow the electric field lines). (c) Exposed to corona ions, but tube located near (controlled spray discharging and extraction). (d) Ions turned off, while tube is near the spray (presence affecting the droplet trajectories). (e) Ions are on, and tube closer. (Better extraction.) $V_{ES} = 4.6$ kV, $V_R = 1.0$ kV, $I_{ES} = 46$ nA, $I_C = -12.0$ μA, $I_{Ext} = -60$ nA, $H = 17.0$ mm, $h = 2.2$ mm, $Q = 0.5$ μl/min. $Q_C = 20$ ml/min $v_{tube} = 5.5$ m/s. The glass urn was removed in these experiments to attain best image quality. Scale bars: 3 mm.

MEK. This polymer solution leads to Coulombic explosions of the droplets, as revealed by the formation of progeny particles (Bodnár, 2016). Therefore, it is suitable to test whether exposure to ions can reduce the droplets' initial charge sufficiently to prevent such explosions. We either sampled the electrospray by collecting it onto a Si wafer (to confirm the existence of progeny particles) or we extracted it by sucking it into an antistatic tube after discharging the spray by corona ions. The tube flow runs through a collection filter, where the collected particles were weighed and inspected by SEM. The filter was housed in either a metal or a plastic filter holder. When a metal holder was used, the Faraday cage electrical current was also monitored during collection (see Materials and Methods). Collections for several tens of minutes were performed, at various test conditions and configurations, which are listed in Table 2.

Fig. 5a shows images of electrospray discharging under different conditions. The sprays in all cases were substantially steady and their shape resembled comparable situations observed with the ethylene glycol sprays (#3.2 and Fig. 4c,e). The Taylor cone was monitored throughout the experiments under brightfield illumination, as in the example of Fig. 5a, to ensure that cone-jet mode was achieved (Rosell-Llompart et al., 2018). Between M.1 and M.2 (3 μl/min) the tube was placed at a height difference of 1 mm, with minimal impact on the shape of the spray plume, which appeared to completely enter the extraction tube. Raising the liquid flow rate from 3 to 5 μl/min (from M.2 to M.3) resulted in a widened spray plume and increase in light scattering. Both these changes are consistent with typical electrospray behavior. The spray plume widens due to electrostatic repulsion in the radial direction, as more charge is injected into the spray. Light scattering increases as the result of increased droplet size (obtained at the higher liquid flow rate).

Raising the corona current I_C threefold between M.3 and M.4 (from −5.4 to −14.8 μA) did not result in appreciable differences in plume shape or scattered light intensity. This is consistent with the fact established earlier in Fig. 2 that the ionic current I_{Ext} reaching the ring region is insensitive to the corona needle current. However, from M.4 to M.5, where H went from 18.5 to 12.0 mm (at constant voltages) to intensify the electric field, the ionic current I_{Ext} (shown in Table 2) had a big effect on the spray shapes (Fig. 5a). In addition to the ionic current increase, H must change the ions' trajectories as they were injected closer to the ring. Therefore, the current flux

Table 2
Parameters and data for the particle collection experiments with polystyrene electrosprays.[a]

Sample Note b	*Q(μl/min)*	*H(mm)*	$I_C(\mu A)$	*Tube radial position (mm)*	$I_{ES}(nA)$ Note c	$I^*_{ES}(nA)$ Note d	$I_R(nA)$	$I_{Ext}(nA)$ Note e	$I'_{Ext}(nA)$ Note f	*Collection time (min)*	*Extraction efficiency, η(%)*	*Filter assembly fraction, η_{FA}(%)*	*Discharge efficiency, ζ(%)*
M.1	3.0	18.5	−5.5	2.0	25	25	−22	−40	−44	41.3	109	89	86
P.1										41.2	108	63	–
M.2	3.0	18.5	−5.4	2.7	25	27	−22	−40	−47	44.6	108	100	93
P.2										44.6	107	81	–
M.3	5.0	18.5	−5.4	2.5	29	43	−19	−40	−58	24.2	102	68	83
P.3										23.0	110	65	–
M.4	5.0	18.5	−14.8	3.3	29	36	−20	−50	−53	12.2	112	79	87
P.4										24.0	107	52	–
M.5	5.0	12.0	−12.4	2.0	30	40	–	−90	–	24.3	111	103	95

[a] In all cases: $V_{ES} = 2.3$ kV, $V_R = 0.9$ kV, $v_{coflow} = 80$ mm/s, $v_{tube} = 5.5$ m/s, $Q_C = 20$ ml/s, $RH < 2\%$.
[b] Metallic (M.x) and plastic (P.x) filter holder.
[c] Measured just before introducing the ions.
[d] Measured during spraying with corona ions present.
[e] Ionic current injected into the spray region estimated from Fig. 2 as a function of V_R and I_C.
[f] Ionic current injected into the spray region estimated according to a charge balance (see text).

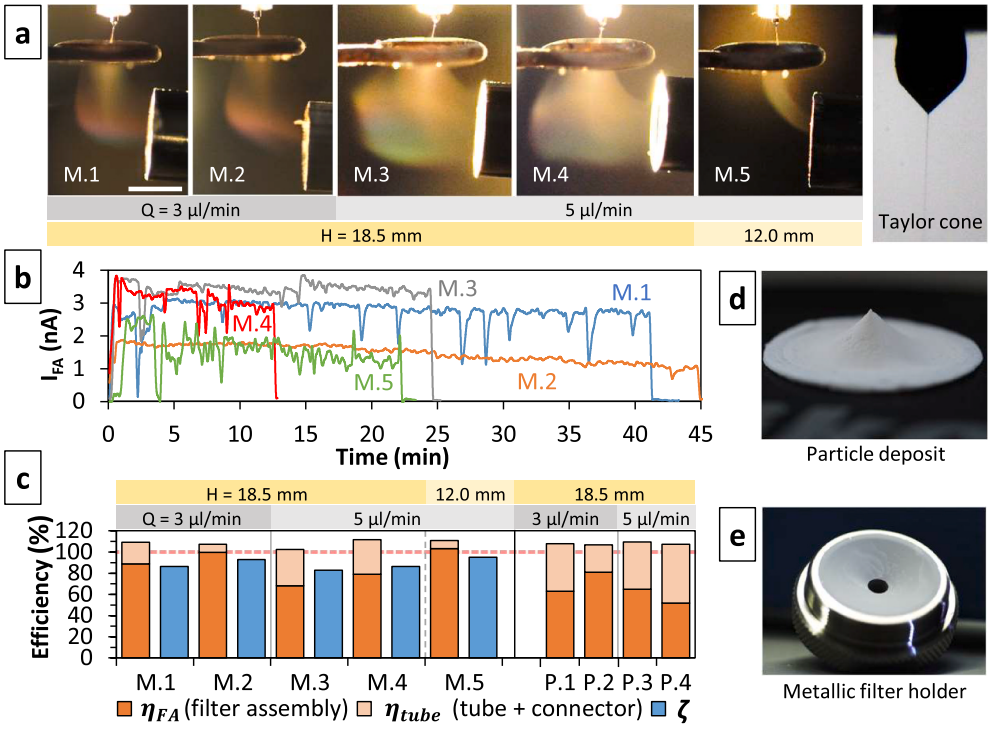

Fig. 5. Polystyrene-MEK solution electrospray neutralization data (3 PS-MEK). (a) Left: Representative snapshots taken during the discharge (scale bar: 3 mm). Right: Taylor cone and jet (b) Faraday-cage electrometer signal I_{FA} corresponding to the residual current carried by the particles. (c) Efficiencies associated to the masses collected on the filter assembly η_{FA} (dark orange) and on the tube and connector η_{tube} (light orange), discharge efficiency ζ (blue bars). (d,e) Examples of particle collections on a 13 mm filter (d) and on metallic filter holder (25 mm) (e). Common parameters for (a–c): $V_{ES} = 2.3$ kV, $V_R = 0.9$ kV, $h = 1.7$ mm, $v_{tube} = 5.5$ m/s, $v_{coflow} = 80$ mm/s. See Table 2 for additional information. (For interpretation of the references to colour in this figure legend, the reader is referred to the Web version of this article.)

(current per unit cross-sectional area) must be much greater in M.5 than in M.4 (or M.3). This explains why H is reduced from M.4 to M.5 the electrospray plume appears to be neutralized closer to the Taylor cone, where the droplet density is higher, the plume is narrower, and therefore the current flux for the droplets is also higher (than would be found further downstream in the absence of ions). In other words, one would expect that in order to discharge the electrospray efficiently, not only the ionic and spray currents, but their associated fluxes should be matched, as well. Note also that for the M.5 run, the plume electrostatic expansion appears to cease (with the spray attaining constant width).

Unlike in the ethylene glycol experiments (previous section), we did not observe liquid accumulation on the electrodes. However, we found small amounts of particles deposited at the entrance of the extraction tube (both on outer and inner walls), as is visible in Fig. 5a and Fig. SI.2 of the Supplementary Information file. Maybe, the particles which had deposited early repelled other particles electrostatically, thus preventing continued deposition.

Finally, it is interesting to compare the ionic current obtained from a charge balance, with the ionic current estimated from the direct measurements shown in Fig. 2. The two values are shown in Table 2, as I'_{Ext} and I_{Ext} respectively. The former is the sum of the current contributions due to the ions only, namely: (i) the ring current (I_R), which is due to the ions (as its value is 0 before the ions are introduced), (ii) the ES capillary current (I^*_{ES}) when the ions are present, which includes the part of the ions which reach the Taylor cone and the ions that combine with the droplets, (iii) decreased by the filter assembly current (I_{FA}), which is the residual droplets' charge which the ions were not able to cancel out: $I'_{Ext} = I_R - (I^*_{ES} - I_{FA})$. The two values in the Table for I_{Ext} are quite similar, which leads to two conclusions: (i) That the droplets are indeed significantly discharged by the capture of ionic charge; and (ii) that the ionic plume spreads significantly, enough to reach the ring.

3.3.1. PS/MEK discharging efficiencies

Fig. 5b shows the time traces of the filter assembly current, I_{FA}, for the same conditions from panel 5a when a metal filter holder was used. These currents were always positive and slowly decreasing with time, with a similar decay rate. Such decay may be due to the slow buildup of charge on the filter, eventually leading to rejection of incoming positively charged particles. When plastic filter holders we used (P.x conditions) the FA currents were erratic, fluctuating around 0 nA (shown in Fig. SI.3); so, these were not used to determine discharging efficiencies. In all cases, the current was always much smaller than I_{ES}, consistent with extensive discharging of the spray by the ions (Table 2). Note that a small but finite residual charge could be desirable to prevent coalescence while the droplets are drying up.

The I_{FA} traces were integrated and used to compute discharging efficiencies ζ by Eq. (3). These are shown in Fig. 5c by blue bars and ranged between 83 and 95%. Incomplete droplet discharging is not surprising because the extent of discharging of the individual droplets must depend on each droplet's exposure to a certain ion flux as it travels through its trajectory, which probably varies for different droplet trajectories. In addition, theoretically, under a constant influx of ions the droplets should eventually reverse sign and achieve a limiting stationary negative charge level. In fact, we cannot rule out the presence of negatively charged particles as I_{FA} is a *net* current.

3.3.2. PS/MEK mass efficiencies (extraction versus filter collection)

Fig. 5c also shows mass collection efficiencies (orange bars) associated with the mass fractions collected on the extraction tube η_{tube} (tube and connector) and on the filter assembly η_{FA} (filter and holder), whose sum equals the extraction efficiency η (Eq. (2)). The filter assembly fraction was systematically larger when a metal filter holder was used, compared to plastic (for otherwise the same conditions). For the metal holder set, the highest two filter collection fractions were observed for conditions M.2 and M.5, which also had the highest discharge efficiencies ζ. At the lowest flow rate, the filter collection efficiency depended on the extraction tube position. On increasing the flow rate from 3 to 5 μl/min, we observed a drop in the filter collection efficiency η_{FA}. This might be attributed to the difficulty of handling an increased spray current and wider spray plume. The filter efficiency increased dramatically when at 5 μl/min we reduced H (condition M.5), for which we think that the ionic and spray current fluxes are matched nearer to the droplet generation zone (see earlier discussion).

The extraction efficiencies η were numerically higher than 100% (102–112%) for all the tested conditions. Ancillary tests indicate as most probable cause the absorption of solvent traces in the polymer matrix of the collected particles. (These and other tests aimed to identify the source of the mass excess are described in the Supplementary File.) Regardless, the important overall conclusion from these data is that the extraction efficiencies η were near 100% in all cases, consistently with the entering of the whole aerosol into the extraction tube observed (Fig. 5a), and with the high discharging ζ (#3.3.1).

3.3.3. Morphologies of the particles collected on filters from PS/MEK sprays

The characteristics of the particle residues observed by SEM reflects whether the droplets suffered the first Coulombic instability (CI) before it is prevented by the strength of the polymer shell forming by solvent drying (Bodnár et al., 2018). First, we imaged the particle residues by SEM to show that in the absence of ions the droplets underwent CI. These are shown in Fig. 6, in panels Si.1 and Si.2, corresponding to collections on Si wafers at flow rates of 3 and 5 μl/min. In both cases, filamented main particles and progeny particles were the predominant, structures, revealing CIs (Almería et al., 2010; Bodnár et al., 2018). This finding agrees with our

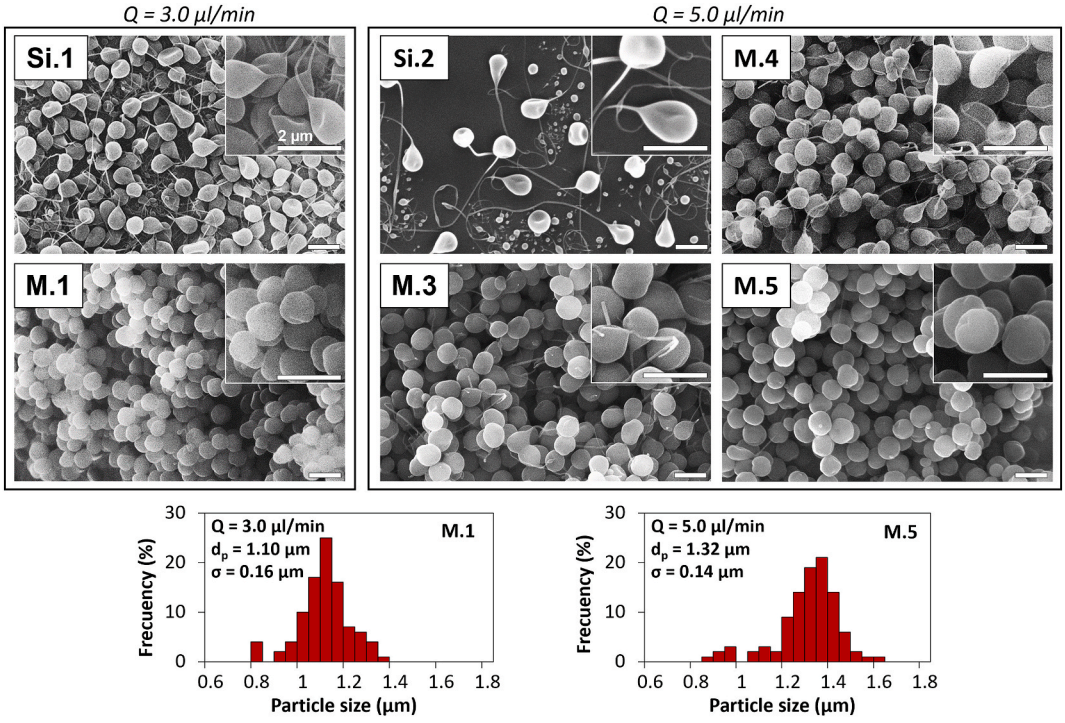

Fig. 6. Comparison of morphology and sizes of PS particles made from 3 PS-MEK solution which were collected either on Si wafer, without corona ions, (conditions Si.1 and Si.2) or on a filter, with corona ions present (conditions M.x, Table 2). Electrode configuration with $h = 1.7$ mm, $H = 18.5$ mm except for M.5 ($H = 12.0$ mm). The filters were housed in the metal holder. Bottom: Particle diameter histograms from 100 particles (each) for the two conditions leading to filament-free particles (M.1 and M.5), where d_p = mean diameter, and σ = standard deviation. All scale bars: 2 μm.

previous work with this solution composition (made with even the same polymer batch) albeit for slightly lower Q of 2 μl/min (Bodnár, 2016).

When the electrospray at 3 μl/min was exposed to the corona ions, particles with globular morphology were instead collected on the filter, as shown in panel M.1 in Fig. 6. On the other hand, similar ion conditions were not as effective on the 5 μl/min spray as shown by the significant fraction of filamentous particles in panel M.3. Although this means that the droplets for this case suffered Coulombic instability, the low residual current, the high discharging efficiency, and the large collection efficiency shown in Fig. 5c (M.3) prove that the electrospray droplets still picked up a significant ionic current. On raising the corona current to −14 μA (M.4) (from −5.5 μA at condition M.3) the particles' morphologies did not vary appreciably from condition M.3. This is clearly consistent with the fact, shown earlier in Fig. 2, that the current injected into the spray does not change much with corona current. Therefore, the neutralizing capacity of the ions was not significantly improved when the corona current was increased.

On the other hand, when the distance H between the ion source and the ring electrode was decreased to 12.0 mm in condition M.5 (from 18.5 mm in M.4), spheroidal particles without filaments were collected (Fig. 6). This reveals that the droplets were electrically discharged early enough to prevent the first Coulombic instability. This finding is consistent with the images of the spray in Fig. 5a, which show that the reduction in H between conditions M.4 and M.5 resulted in a significant narrowing of the spray plume and, probably, an upstream shifting of the discharging zone (as argued earlier).

Importantly, the addition of corona ions to the spray did not apparently change the sizes of the particles (comparing Si.x and M.x conditions in Fig. 6). This proves that the ions did not interfere with the jet formation process. At least, the jet diameter at the jet breakup position did not change appreciably, because the particle size remains approximately the same. However, the electrical current at the ES capillary increased when the ions were introduced (from I_{ES} to I_{ES}^{*} as shown in Table 2). This has been seen for many conditions. The current increase could be due to (i) ions reaching the Taylor cone, or (ii) ions reducing the space charge of the spray cloud (the net charge due to the ion and the spray clouds), thus increasing the electrical field at the Taylor cone and the current (partially offset by the down-adjustment of voltage explained in #2.4). Regardless, the fluid dynamics of the jet formation was not

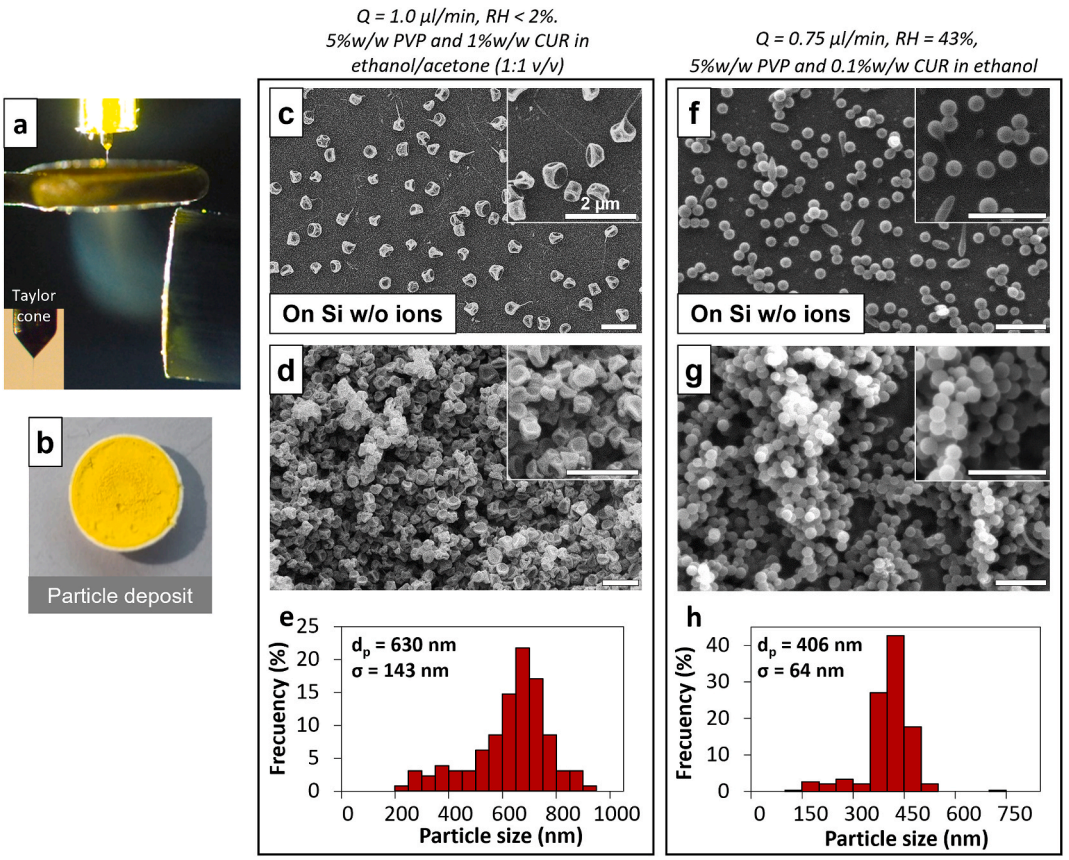

Fig. 7. Morphology and sizes of particles made from PVP-curcumin solutions. (a) Snapshot of a steady electrospray during discharging and extraction, inset showing the Taylor cone. (b) Example of particle deposit on filter (25 mm dia.). (c,d) SEM images of particles from solution 1CUR-5PVP sprayed at $Q = 1.0$ μl/min, $RH < 2\%$, $h = 1.2$ mm, $H = 17.0$ mm, as collected on a Si wafer without ions (c) and on a filter (d). (e) Particle size histogram for (d) from 129 particles. (f,g) SEM images of particles from solution 0.1CUR-5PVP sprayed at $Q = 0.75$ μl/min, $h = 1.0$ mm, $H = 27.0$ mm, $RH = 43\%$, as collected on Si wafer without ions (f) and on filter (g). (h) Particle size histogram for (g) from 300 particles. For (e,h), d_p = particle mean diameter, σ = standard deviation. All scale bars: 2 μm.

perturbed by the ions enough to change the jet width at breakup. If it had, a change would probably have been seen in the particle size between the Si-wafer and filter particle collections of Fig. 6.

The previous argument assumes the known fact that the length of jet transforming into a single droplet (the jet breakup wavelength) is fairly insensitive to how much electrical charge it carries (which would decrease if ions hit the jet) (Gamero-Castaño & Hruby, 2002). Nonetheless, the arrival of ions to the jet cannot be ruled out just from the insensitivity of particle size to them. This is due to two opposing tendencies. On the one hand, a significant deposition of ions on the jet near its breakup region would lower the net electrical surface charge, thus reducing the normal electrical stresses that oppose the surface tension stresses. As a consequence, the jet break-up process would be accelerated, happening "earlier", i.e., further upstream (as demonstrated with electrospinning jets by Fong et al., 1999; see also Saville, 1971). This would cause the breakup of the jet in a region where it is thicker, thus resulting in slightly bigger particles. On the other hand, ions reaching the jet (and the spray) would also reduce the net charge on the jet (and the spray). Therefore, the electrical potential would be lowered at the site of ion arrival, thus intensifying the axial component of the electrical field, which is responsible for accelerating the charged jet. Therefore, its thinning rate would be increased, resulting in a thinner jet. Understanding the relative importance of these two tendencies is beyond the scope of this work. Nonetheless, we can conclude that if ions landed on the jet in our experiments, they did not appreciably affect the size of the jet at its breakup point.

Fig. 6 also shows the particle size histograms of the particles collected on filters for the cases leading to globular (filament-free) particles: M1 and M5. The particles were uniformly sized and shaped at these conditions. Particle diameter count means increased slightly with flow rate from 1.10 μm at 3 μl/min (M.1) to 1.32 μm at 5 μl/min (M.5), while the standard deviations were similar. This increase in particle size with flow rate reflects the "scaling-law" dependence of droplet size with flow rate for which particle volume varies approximately linearly with solution flow rate (Rosell-Llompart et al., 2018).

Some particles landed on the inside of the filter holder cap (Fig. 5e), and for selected conditions (M.1, M.3, M.5) we inspected them by SEM, finding that a significant fraction of the particles had filaments. This may indicate that such particles either initially carried more charge or were not as efficiently discharged as those landing on the filter. The SEM images of the filter holder particles are shown in the Supplementary Information file (Fig. SI.4).

3.4. Curcumin-loaded PVP particles from discharged electrosprays

We have also applied this methodology to produce polymer-model drug particles made of polyvinylpyrrolidone (PVP) and curcumin (CUR), as a carrier-drug model. We chose a composition of 5% w/w PVP and 1% w/w CUR in ethanol/acetone (1:1 v/v) as this is a relatively dilute solution capable of producing small particles. Using $h = 1.2$ mm and $H = 17.0$ mm, we established the cone-jet mode (Fig. 7a) at a liquid flow rate of 1.0 μl/min with an electrospray current of 32 nA. The particles collected on Si wafer without ionic discharging were filamentous, as shown in Fig. 7c, whereas the particles on the filter after discharging were mostly globular, with a minor presence of filaments, as shown in Fig. 7d. The size distribution on the filter particles is monomodal and homogeneous, with count mean (Martin) diameter and standard deviation of 630 ± 143 nm (Fig. 7e). The collection efficiencies η in two independent experiments were 100% and 97%, where the filter assembly fractions η_{FA} were 90% and 76% for collection times of 64 and 44 min, respectively. The averaged value for the residual current was +3.0 nA in both cases, corresponding to discharging efficiencies ζ of 90% and 88%.

We performed an ancillary experiment at elevated ambient humidity of 43–53% RH (after lifting the chamber glass urn), using a solution of 5% w/w PVP and 0.1% w/w CUR in ethanol, at liquid flow rate $Q = 0.75$ μl/min, and with $h = 1.0$ mm and $H = 27.0$ mm. Without ions, on a Si wafer we collected submicrometric particles having mixed geometries: globular, spherical, or elongated (Fig. 7f). With ions, a 20 min filter collection resulted in similarly sized nearly spherical and monomodal nanoparticles (Fig. 7g), with a narrow particle size distribution with count mean and standard deviation of 406 ± 64 nm, shown in Fig. 7h.

Just as seen before in the PS experiments (section 3.3.3), here the ions did not change the size of the particles, so we conclude that the ions did not affect the jet breakup pattern. The electrospray current did not change when the ions were added during the low relative humidity experiments ($I^*_{ES} = I_{ES} = 32$ nA), while I_R went from 0 to −3 nA.

4. Conclusions

We demonstrate a continuous process for the effective prevention of Coulombic instabilities in electrospray droplets' by reducing their charge in situ using opposite-polarity unipolar ions from a corona source. In our design a fraction of the current produced in a negative corona discharge is introduced axially into the electrospray, approximately matching the electrospray current. The discharged aerosol is then extracted orthogonally by an antistatic extraction tube, and dry particles are then collected on a filter where their residual electrical charge is continuously measured. Electrospraying in capillary-ring configuration allows us to stabilize the spraying process independently from the presence of ions. Meanwhile, the spray-ions interactions are controlled mainly by the voltage difference between the ring electrode and the ion source. Droplet flyback towards the ring can be prevented robustly over a wide range of ring voltages. A key methodological aspect related to the corona generation is our use of current regulation at the power supply (as opposed to voltage regulation) to stabilize the corona.

Stable electrospray discharging allowed the continuous extraction of the discharged droplets/particles into an antistatic tube with near 100% efficiency. The removal of particles by a proximal antistatic tube is critical to the stability of the process, as it prevents the charge reversal of the droplets with consequent migration toward the Taylor cone and/or agglomeration events with other particles.

We have found that the geometrical and electrostatic parameters are key to maximize droplet discharging and minimize droplet

loss.

We found that the distance between the ring electrode and ion source controlled the location where the ions interacted with the droplets. Reducing this distance intensified the electric field, it increased ionic current flux near the axis (current/area), causing the upstream shift of the droplet discharging by the ions, and resulting in higher extraction efficiency, filter collection fraction, and more globular particles. Therefore, an ion stream with higher current flux seems capable of matching the spray current nearer to the Taylor cone, where it has a higher current flux as well. This finding is significant because it suggests that ultra-compact systems based on this principle could be developed.

For the fraction reaching the (metal) filter assembly, the electrical discharging is greater than 80%. The presence of residual electric charge on the extracted droplets/particles may explain why the mass on the filter is lower when a plastic filter holder is used than when a metal one is used (when electrical fields are weaker). The extracted aerosols had a significant residual charge (less than 20% the electrospray current). This suggests that dissimilar degrees of discharging are attained by droplets following different trajectories in the spray. Nonetheless, in future applications of this method, a small residual electrostatic charge on the extracted particles could be beneficial to prevent agglomeration in the aerosol phase.

Regarding particle size and shape, the discharging process did not affect the overall size of the electrospray particles (droplet residues), while greatly reducing the fraction of elongated/filamentous particles (which is a typical signature of Coulombic instabilities). Particle globularity was positively correlated with collection and discharging efficiencies. The size distributions for the particles collected on the filters were monomodal and homogeneous, with small relative standard deviations (as small as 10.6%).

In sum, the use of corona ions significantly expands the range of polymer concentrations over which globular particles with monomodal size distribution can be made by electrospray. We hope that, in addition, the ability to transport the particles away from the electrospray region will also inspire studies where the particles are subject to secondary in-line thermal or chemical post-processing of the particles in aerosol form.

Declaration of competing interest

The authors declare that they have no known competing financial interests or personal relationships that could have appeared to influence the work reported in this paper.

Acknowledgements

We want to thank Dr. Christian Lübbert (FAU, Germany) and Prof. Francisco Higuera (UPM, Spain) for fruitful discussions. This project has received funding from the Spanish Government through grants PGC2018-099687-B-I00 (MCI/AEI/FEDER, UE) and DPI2015-68969-P (MINECO/FEDER, UE), and from the Catalan Government through grant 2017SGR1516 (AGAUR). E. Barbero acknowledges the Spanish Government scholarship BES-2016-077914 (MINECO/AEI/FEDER, UE).

Appendix A. Supplementary data

Supplementary data to this article can be found online at https://doi.org/10.1016/j.jaerosci.2021.105909.

References

Ali, A., Zaman, A., Sayed, E., Evans, D., Morgan, S., Samwell, C., Hall, J., Sohail Arshad, M., Simgh, N., Qutachi, O., Chang, M.-W., & Ahmad, Z. (2021). Electrohydrodynamic atomisation driven design and engineering of opportunistic particulate systems for applications in drug delivery, therapeutics and pharmaceutics. *Advanced Drug Delivery Reviews, 176*, 113788. https://doi.org/10.1016/j.addr.2021.04.026

Almería, B., Deng, W., Fahmy, T. M., & Gomez, A. (2010). Controlling the morphology of electrospray-generated PLGA microparticles for drug delivery. *Journal of Colloid and Interface Science, 343*(1), 125–133. https://doi.org/10.1016/j.jcis.2009.10.002

Almería, B., Fahmy, T. M., & Gomez, A. (2011). A multiplexed electrospray process for single-step synthesis of stabilized polymer particles for drug delivery. *Journal of Controlled Release, 154*(2), 203–210. https://doi.org/10.1016/j.jconrel.2011.05.018

Almería, B., & Gomez, A. (2014). Electrospray synthesis of monodisperse polymer particles in a broad (60 nm-2 μm) diameter range: Guiding principles and formulation recipes. *Journal of Colloid and Interface Science, 417*, 121–130. https://doi.org/10.1016/j.jcis.2013.11.037

Arumugham-Achari, A. K., Grifoll, J., & Rosell-Llompart, J. (2013). Two-way coupled numerical simulation of electrospray with induced gas flow. *Journal of Aerosol Science, 65*, 121–133. https://doi.org/10.1016/j.jaerosci.2013.07.005

Bocanegra, R., Galán, D., Márquez, M., Loscertales, I. G., & Barrero, A. (2005). Multiple electrosprays emitted from an array of holes. *Journal of Aerosol Science, 36*(12), 1387–1399. https://doi.org/10.1016/j.jaerosci.2005.04.003

Bock, N., Dargaville, T. R., & Woodruff, M. A. (2012). Electrospraying of polymers with therapeutic molecules: State of the art. *Progress in Polymer Science, 37*(11), 1510–1551. https://doi.org/10.1016/j.progpolymsci.2012.03.002

Boda, S. K., Li, X., & Xie, J. (2018). Electrospraying an enabling technology for pharmaceutical and biomedical applications: A review. *Journal of Aerosol Science, 125*, 164–181. https://doi.org/10.1016/j.jaerosci.2018.04.002

Bodnár, E. (2016). *Electrospraying of polymer solutions for the generation of micro-particles, nanostructures, and granular films*. Universitat Rovira i Virgili). Retrieved from http://www.tdx.cat/handle/10803/379820.

Bodnár, E., Grifoll, J., & Rosell-Llompart, J. (2018). Polymer solution electrospraying: A tool for engineering particles and films with controlled morphology. *Journal of Aerosol Science, 125*, 93–118. https://doi.org/10.1016/j.jaerosci.2018.04.012

Bodnár, E., & Rosell-Llompart, J. (2013). Growth dynamics of granular films produced by electrospray. *Journal of Colloid and Interface Science, 407*, 536–545. https://doi.org/10.1016/j.jcis.2013.06.013

Bornschein, R. E., & Ruotolo, B. T. (2015). Ion mobility-mass spectrometry of charge-reduced protein complexes reveals general trends in the collisional ejection of compact subunits. *Analyst, 140*(20), 7020–7029. https://doi.org/10.1039/c5an01242b

Campuzano, I. D. G., & Schnier, P. D. (2013). Coupling electrospray corona discharge, charge reduction and ion mobility mass spectrometry: From peptides to large macromolecular protein complexes. *International Journal for Ion Mobility Spectrometry, 16*(1), 51–60. https://doi.org/10.1007/s12127-013-0120-x

Castillo, J. L., Martin, S., Rodriguez-Perez, D., Higuera, F. J., & Garcia-Ybarra, P. L. (2018). Nanostructured porous coatings via electrospray atomization and deposition of nanoparticle suspensions. *Journal of Aerosol Science, 125*, 148–163. https://doi.org/10.1016/j.jaerosci.2018.03.004

Ciach, T. (2006). Microencapsulation of drugs by electro-hydro-dynamic atomization. *International Journal of Pharmaceutics, 324*(1), 51–55. https://doi.org/10.1016/j.ijpharm.2006.06.035

Ciach, T. (2007). Application of electro-hydro-dynamic atomization in drug delivery. *Journal of Drug Delivery Science and Technology, 17*(6), 367–375. https://doi.org/10.1016/S1773-2247(07)50076-6

Cloupeau, M. (1994). Recipes for use of EHD spraying in cone-jet mode and notes on corona discharge effects. *Journal of Aerosol Science, 25*(6), 1143–1157. https://doi.org/10.1016/0021-8502(94)90206-2

Davies, L. A., Hannavy, K., Davies, N., Pirrie, A., Coffee, R. A., Hyde, S. C., & Gill, D. R. (2005). Electrohydrodynamic comminution: A novel technique for the aerosolisation of plasmid DNA. *Pharmaceutical Research, 22*(8), 1294–1304. https://doi.org/10.1007/s11095-005-5268-6

Deng, W., Klemic, J. F., Li, X., Reed, M. A., & Gomez, A. (2006). Increase of electrospray throughput using multiplexed microfabricated sources for the scalable generation of monodisperse droplets. *Journal of Aerosol Science, 37*(6), 696–714. https://doi.org/10.1016/j.jaerosci.2005.05.011

Duft, D., Achtzehn, T., Müller, R., Huber, B. a, & Leisner, T. (2003). Coulomb fission: Rayleigh jets from levitated microdroplets. *Nature, 421*(6919), 128. https://doi.org/10.1038/421128a

Ebeling, D. D., Westphall, M. S., Scalf, M., & Smith, L. M. (2000). Corona discharge in charge reduction electrospray mass spectrometry. *Analytical Chemistry, 72*(21), 5158–5161. Retrieved from http://pubs.acs.org/doi/abs/10.1021/ac000559h.

Ebeling, D. D., Westphall, M. S., Scalf, M., & Smith, L. M. (2001). A cylindrical capacitor ionization source: Droplet generation and controlled charge reduction for mass spectrometry. *Rapid Communications in Mass Spectrometry, 15*(6), 401–405. https://doi.org/10.1002/rcm.245

Echegoyen, Y., Fabra, M. J., Castro-Mayorga, J. L., Cherpinski, A., & Lagaron, J. M. (2017). High throughput electro-hydrodynamic processing in food encapsulation and food packaging applications : Viewpoint. *Trends in Food Science & Technology, 60*, 71–79. https://doi.org/10.1016/j.tifs.2016.10.019

Fenn, J. B. (2003). Electrospray wings for molecular elephants (Nobel lecture). *Angewandte Chemie International Edition, 42*(33), 3871–3894. https://doi.org/10.1002/anie.200300605

Fong, H., Chun, I., & Reneker, D. H. (1999). Beaded nanofibers formed during electrospinning. *Polymer, 40*(16), 4585–4592. https://doi.org/10.1016/S0032-3861(99)00068-3

Gamero-Castaño, M., & Hruby, V. (2002). Electric measurements of charged sprays emitted by cone-jets. *Journal of Fluid Mechanics, 459*, 245–276. https://doi.org/10.1017/S002211200200798X

Gañán-Calvo, A. M., López-Herrera, J. M., Herrada, M. A., Ramos, A., & Montanero, J. M. (2018). Review on the physics of electrospray: From electrokinetics to the operating conditions of single and coaxial Taylor cone-jets, and AC electrospray. *Journal of Aerosol Science, 125*, 32–56. https://doi.org/10.1016/j.jaerosci.2018.05.002

Gomez, A., & Tang, K. (1994). Charge and fission of droplets in electrostatic sprays. *Physics of Fluids, 6*(1), 404–414. https://doi.org/10.1063/1.868037

Higuera, F. J. (2012). Eulerian model of a dilute spray of charged droplets. *Journal of Aerosol Science, 48*, 34–45. https://doi.org/10.1016/j.jaerosci.2012.01.008

Higuera, F. J. (2016). Neutralization of a spray of electrically charged droplets by a corona discharge. *Journal of Fluid Mechanics, 801*, 130–149. https://doi.org/10.1017/jfm.2016.449

Hogan, C. J., & Biswas, P. (2008). Porous film deposition by electrohydrodynamic atomization of nanoparticle sols. *Aerosol Science and Technology, 42*(1), 75–85. https://doi.org/10.1080/02786820701787951

Hogan, C. J., Yun, K. M., Chen, D. R., Lenggoro, I. W., Biswas, P., & Okuyama, K. (2007). Controlled size polymer particle production via electrohydrodynamic atomization. *Colloids and Surfaces A: Physicochemical and Engineering Aspects, 311*(1–3), 67–76. https://doi.org/10.1016/j.colsurfa.2007.05.072

Ijsebaert, J. C., Geerse, K. B., Marijnissen, J. C. M., Lammers, J. W., & Zanen, P. (2001). Electro-hydrodynamic atomization of drug solutions for inhalation purposes. *Journal of Applied Physiology, 91*(6), 2735–2741. https://doi.org/10.1152/jappl.2001.91.6.2735

Jafari, S. M., Arpagaus, C., Cerqueira, M. A., & Samborska, K. (2021). Nano spray drying of food ingredients; materials, processing and applications. *Trends in Food Science & Technology, 109*, 632–646.

Jaworek, A. (2007a). Electrospray droplet sources for thin film deposition. *Journal of Materials Science, 42*(1), 266–297. https://doi.org/10.1007/s10853-006-0842-9

Jaworek, A. (2007b). Micro- and nanoparticle production by electrospraying. *Powder Technology, 176*(1), 18–35. https://doi.org/10.1016/j.powtec.2007.01.035

Jaworek, A., Sobczyk, A. T., & Krupa, A. (2018). Electrospray application to powder production and surface coating. *Journal of Aerosol Science, 125*, 57–92. https://doi.org/10.1016/j.jaerosci.2018.04.006

Kelder, E. M., Marijnissen, J. C. M., & Karuga, S. W. (2018). EDHA for energy production, storage and conversion devices. *Journal of Aerosol Science, 125*, 119–147. https://doi.org/10.1016/j.jaerosci.2018.04.011

Khalifehei, M., & Higuera, F. J. (2020). Neutralization of an electrospray by a corona discharge. *Journal of Aerosol Science, 145*, 105547. https://doi.org/10.1016/j.jaerosci.2020.105547

Lenggoro, I. W., Okuyama, K., Fernández de la Mora, J., & Tohge, N. (2000). Preparation of ZnS nanoparticles by electrospray pyrolysis. *Journal of Aerosol Science, 31*(1), 121–136. https://doi.org/10.1016/S0021-8502(99)00534-0

Li, D., Marquez, M., & Xia, Y. (2007). Capturing electrified nanodroplets under Rayleigh instability by coupling electrospray with a sol-gel reaction. *Chemical Physics Letters, 445*(4–6), 271–275. https://doi.org/10.1016/j.cplett.2007.07.090

Malamatari, M., Charisi, A., Malamataris, S., Kachrimanis, K., & Nikolakakis, I. (2020). Spray drying for the preparation of nanoparticle-based drug formulations as dry powders for inhalation. *Processes, 8*(7), 788. https://doi.org/10.3390/pr8070788

Meesters, G. M. H., Vercoulen, P. H. W., Marijnissen, J. C. M., & Scarlett, B. (1992). Generation of micron-sized droplets from the Taylor cone. *Journal of Aerosol Science, 23*(1), 37–49. https://doi.org/10.1016/0021-8502(92)90316-N

Meng, F., Jiang, Y., Sun, Z., Yin, Y., & Li, Y. (2009). Electrohydrodynamic liquid atomization of biodegradable polymer microparticles: Effect of electrohydrodynamic liquid atomization variables on microparticles. *Journal of Applied Polymer Science, 113*(1), 526–534. https://doi.org/10.1002/app.30107

Mustika, W. S., Hapidin, D. A., Saputra, C., & Munir, M. M. (2021). Dual needle corona discharge to generate stable bipolar ion for neutralizing electrosprayed nanoparticles. *Advanced Powder Technology, 32*(1), 166–174. https://doi.org/10.1016/j.apt.2020.11.026

Nandiyanto, A. B. D., & Okuyama, K. (2011). Progress in developing spray-drying methods for the production of controlled morphology particles: From the nanometer to submicrometer size ranges. *Advanced Powder Technology, 22*(1), 1–19. https://doi.org/10.1016/j.apt.2010.09.011

Nguyen, D. N., Clasen, C., & Van den Mooter, G. (2016). Pharmaceutical applications of electrospraying. *Journal of Pharmaceutical Sciences, 105*(9), 2601–2620. https://doi.org/10.1016/j.xphs.2016.04.024

Noakes, T. J., Pavey, I. D., Bray, D., & Rowe, R. C. (1989). Retrieved from https://pdfpiw.uspto.gov/.piw?PageNum=0&docid=04829996. Patent No. US Patent 4,829,996.

Okuyama, K., & Lenggoro, W. W. (2003). Preparation of nanoparticles via spray route. *Chemical Engineering Science, 58*(3–6), 537–547. https://doi.org/10.1016/S0009-2509(02)00578-X

Rosell-Llompart, J., & Gañán-Calvo, A. M. (2008). Turbulence in pneumatic flow focusing and flow blurring regimes. *Physical Review, 77*(3), 36321. https://doi.org/10.1103/PhysRevE.77.036321

Rosell-Llompart, J., Grifoll, J., & Loscertales, I. G. (2018). Electrosprays in the cone-jet mode: From Taylor cone formation to spray development. *Journal of Aerosol Science, 125*, 2–31. https://doi.org/10.1016/j.jaerosci.2018.04.008

Rostamabadi, H., Falsafi, S. R., Rostamabadi, M. M., Assadpour, E., & Jafari, S. M. (2021). Electrospraying as a novel process for the synthesis of particles/nanoparticles loaded with poorly water-soluble bioactive molecules. *Advances in Colloid and Interface Science, 290*, 102384. https://doi.org/10.1016/j.cis.2021.102384

Rulison, A. J., & Flagan, R. C. (1994). Synthesis of yttria powders by electrospray pyrolysis. *Journal of the American Ceramic Society, 77*(12), 3244–3250. https://doi.org/10.1111/j.1151-2916.1994.tb04577.x

Saville, D. A. (1971). Stability of electrically charged viscous cylinders. *Physics of Fluids, 14*(6), 1095–1099. https://doi.org/10.1063/1.1693569

Saville, D. A. (1997). Electrohydrodynamics: The Taylor-Melcher leaky dielectric model. *Annual Review of Fluid Mechanics, 29*(1), 27–64. https://doi.org/10.1146/annurev.fluid.29.1.27

Sochorakis, N., Grifoll, J., & Rosell-Llompart, J. (2019). Scaling up of extractor-free electrosprays in linear arrays. *Chemical Engineering Science, 195*, 281–298. https://doi.org/10.1016/j.ces.2018.09.006

Sosnik, Alejandro, & Seremeta, Katia P. (2015). Advantages and challenges of the spray-drying technology for the production of pure drug particles and drug-loaded polymeric carriers. *Advances in Colloid and Interface Science, 223*, 40–54. https://doi.org/10.1016/j.cis.2015.05.003

Suhendi, A., Nandiyanto, A. B. D., Munir, M. M., Ogi, T., Gradon, L., & Okuyama, K. (2013). Self-assembly of colloidal nanoparticles inside charged droplets during spray-drying in the fabrication of nanostructured particles. *Langmuir, 29*(43), 13152–13161. https://doi.org/10.1021/la403127e

Sverdlov Arzi, R., & Sosnik, A. (2018). Electrohydrodynamic atomization and spray-drying for the production of pure drug nanocrystals and co-crystals. *Advanced Drug Delivery Reviews, 131*, 79–100. https://doi.org/10.1016/j.addr.2018.07.012

Tang, K., & Gomez, A. (1994). Generation by electrospray of monodisperse water droplets for targeted drug delivery by inhalation. *Journal of Aerosol Science, 25*(6), 1237–1249. https://doi.org/10.1016/0021-8502(94)90212-7

Tang, J., & Gomez, A. (2017). Controlled mesoporous film formation from the deposition of electrosprayed nanoparticles. *Aerosol Science and Technology, 51*(6), 755–765. https://doi.org/10.1080/02786826.2017.1303573

Tang, J., Liu, W., Wang, H., & Gomez, A. (2016). High performance metal oxide–graphene hybrid nanomaterials synthesized via opposite-polarity electrosprays. *Advanced Materials, 28*(46), 10298–10303. https://doi.org/10.1002/adma.201603339

Tang, J., Wang, H., & Gomez, A. (2017). Controlled nanoparticle synthesis via opposite-polarity electrospray pyrolysis. *Journal of Aerosol Science, 113*, 201–211. https://doi.org/10.1016/j.jaerosci.2017.07.001

Uecker, J. C., Tepper, G. C., & Rosell-Llompart, J. (2010). Ion-assisted collection of Nylon-4,6 electrospun nanofibers. *Polymer, 51*(22), 5221–5228. https://doi.org/10.1016/j.polymer.2010.08.057

Vehring, R., Snyder, H., & Lechuga-Ballesteros, D. (2020). Spray drying. In *Drying technologies for biotechnology and pharmaceutical applications* (pp. 179–216). Wiley-VCHVerlag GmbH& Co. KGaA. https://doi.org/10.1002/9783527802104.ch7.

Xie, J., Lim, L. K., Phua, Y., Hua, J., & Wang, C. H. (2006). Electrohydrodynamic atomization for biodegradable polymeric particle production. *Journal of Colloid and Interface Science, 302*(1), 103–112. https://doi.org/10.1016/j.jcis.2006.06.037

Xie, J., Marijnissen, J. C. M., & Wang, C. H. (2006). Microparticles developed by electrohydrodynamic atomization for the local delivery of anticancer drug to treat C6 glioma in vitro. *Biomaterials, 27*(17), 3321–3332. https://doi.org/10.1016/j.biomaterials.2006.01.034

Xie, J., & Wang, C.-H. (2007). Encapsulation of proteins in biodegradable polymeric microparticles using electrospray in the Taylor cone-jet mode. *Biotechnology and Bioengineering, 97*(5), 1278–1290. https://doi.org/10.1002/bit.21334

Yurkstas, E. P., & Meisenzehl, C. J. (1964). Solid homogeneous aerosol production by electrical atomization. AEC research and development report UR-652. Retrieved from https://pubmed.ncbi.nlm.nih.gov/14242770/.

Yurteri, C. U., Hartman, R. P. A., & Marijnissen, J. C. M. (2010). Producing pharmaceutical particles via electrospraying with an emphasis on nano and nano structured particles - a review. *KONA Powder and Particle Journal, 28*, 91–115. https://doi.org/10.14356/kona.2010010

Zimlich, W., Ding, J., Busick, D., Pham, S., Palmer, D., & Placke, M. (2002). Development of multiple clinical and commercial applications using mystic inhalation delivery technologies. In R. Dalby, P. Byron, J. Peart, & S. Farr (Eds.), *Respiratory drug delivery VIII* (pp. 363–366). Retrieved from https://www.rddonline.com/publications/proceedings/index.php.